# Nanohybrid Liposomal Cerasomes with Good Physiological Stability and Rapid Temperature Responsiveness for High Intensity Focused Ultrasound Triggered Local Chemotherapy of Cancer

**Xiaolong Liang,[†] Jing Gao,[‡] Lingdong Jiang,[§] Jianwen Luo,[‡] Lijia Jing,[§] Xiaoda Li,[§] Yushen Jin,[§] and Zhifei Dai*,[†]**

[†]Department of Biomedical Engineering, College of Engineering, Peking University, Beijing 100871, China, [‡]Department of Biomedical Engineering, School of Medicine, Tsinghua University, Beijing 100871, China, and [§]School of Life Science and Technology, Harbin Institute of Technology, Harbin 150080, China

**ABSTRACT** The high intensity focused ultrasound (HIFU) and thermosensitive cerasomes (HTSCs) were successfully assembled by employing cerasome-forming lipid (CFL) in combination with the component lipids of conventional low temperature sensitive liposomes (LTSLs) including 1,2-dipalmitoyl-*sn*-glycero-3-phosphocholine (DPPC), 1,2-distearoyl-*sn*-glycero-3-phosphoethanolamine-*N*-[methoxy(polyethylene glycol)-2000] (DSPE-PEG-2000) and 1-stearoyl-2-hydroxy-*sn*-glycero-3-phosphocholine (MSPC). The HTSCs showed spherical shape with a mean diameter around 200 nm, exhibiting good biocompatibility. Both hydrophilic and lipophilic drugs can be efficiently encapsulated into HTSCs. In addition, the release rate of HTSCs could be conveniently adjusted by varying the molar ratios of CFL to DPPC. The drug loaded HTSCs showed much longer blood circulation time (half-life >8.50 ± 1.49 h) than conventional LTSLs (0.92 ± 0.17 h). An *in vitro* study demonstrated that the drug loaded HTSCs are highly stable at 37 °C and show a burst release at 42 °C, providing a capability to act synergistically against tumors. We found that the HTSCs with a proportion of 43.25% of CFL could release more than 90% hydrophilic drugs in 1 min at an elevated temperature of 42 °C generated by HIFU exposure. After intravenous injection of doxorubicin (DOX) loaded HTSCs at 5 mg DOX/kg, followed by double HIFU sonication, the tumor growth of the adenocarcinoma (MDA-MB-231) bearing mice could be significantly inhibited. Therefore, the drug loaded HTSCs combined with HIFU hold great potential for efficient local chemotherapy of cancer due to the ability to deliver high concentration of chemotherapy drugs directly to the tumor, achieve maximum therapeutic efficacy and minimal side effects, and avoid the damage to the healthy tissues caused by systemic administration of drugs.

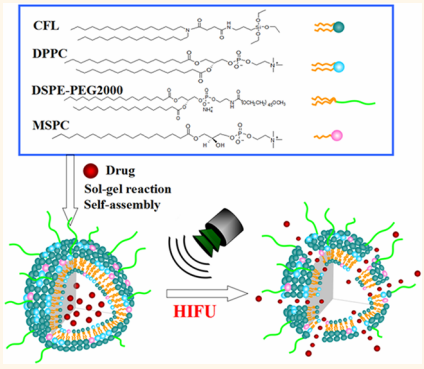


**KEYWORDS:** cerasomes · triggered drug release · high intensity focused ultrasound · local chemotherapy · thermosensitive liposome

Chemotherapy is one of the most common treatment modalities of a variety of cancers.[1−5] The mechanism of many chemotherapeutic drugs currently used for killing cancer cells is based on cytotoxic effects. However, one of the main drawbacks of this therapy is that the most commonly used anticancer drugs are not specifically toxic to tumor cells and are toxic to all tissues they contact.[1,2] Because of the low selectivity of the anticancer drugs to the cancer cells, the dose of drug required to achieve clinically effective cytotoxicity in tumors often causes severe damage to surrounding healthy cells, resulting in undesirable side effects that limit the dose and therapeutic window.[1,2] In addition, the efficacy of free chemotherapeutic agents is also hampered by multidrug resistance.[3,4]

To overcome these problems, a variety of drug nanocarriers that are triggered by stimuli (*i.e.*, pH, enzyme, temperature, and light) have been developed to enhance accumulation in tumor tissues and cells, decrease systemic toxicity, and increased maximum tolerated dosages.[6−12] Drug nanocarriers can accumulate in tumors through passive targeting mechanisms

* Address correspondence to zhifei.dai@pku.edu.cn.

Received for review September 10, 2014 and accepted January 19, 2015.

**Published online January 19, 2015**
**10.1021/nn507482w**

known as the enhanced permeability and retention (EPR) effect,[13,14] active targeting with specific antibodies or other ligands[15] and endothelial cell leakiness effect called NanoEL effect.[16,17] Among the stimuli-responsive drug delivery systems, thermal triggering takes a unique advantage according to the controllability of the temperature at the desired location and time by applying an external biomedical device system such as near-infrared light,[18] radio frequency,[19] microwave,[20] and high intensity focused ultrasound (HIFU).[21−23]

Liposomes acting as excellent nanocarriers of therapeutic agents have attracted intensive interests due to their capability to circumvent multidrug resistance and elicit less host immune response.[24−31] One of the most effective way to reduce unfavorable side effects while treating cancer patients is the employment of temperature sensitive liposome (TSL) in combination with mild hyperthermia (39−42 °C), which can effectively increase the intratumoral drug concentration to circumvent multidrug resistance and elicit less host immune response.[27−29,32−39] HIFU beam can be collimated into a tight focal spot in the millimeter scale at a distance from its source to produce the required high temperature elevations for thermal ablation and direct tumor destruction,[40,41] and HIFU-mediated drug delivery could noninvasively enhance the site-specific delivery of therapeutic agents to targeted tumors by providing nonlethal temperature elevation and increasing cell membrane permeability.[21−23,42−48] Compared with the other heating methods, HIFU is advantageous as a localized stimulus tool since it can propagate into deep tissue and specifically focus into the target.[40,41] Therefore, many researchers are currently investigating the temperature-induced drug delivery technique based on HIFU and low temperature sensitive liposomes (LTSLs), which were prepared by incorporation of the temperature-sensitive component, such as 1-stearoyl-2- hydroxy-*sn*-glycero-3-phosphocholine (MSPC).[42−48]

An ideal drug nanocarrier should be stable enough during blood circulation and give a rapid release of high concentrations of active drug after reaching targeted region. However, it is not easy to achieve both rapid temperature responsiveness and good blood stability since these two elements are apparently different. For example, the insufficient morphological stability of liposomes may limit their applications in drug delivery and controlled release.[49,50] The interactions between liposomes and plasma proteins *via* electrostatic, hydrophobic, and van der Waals may result in destabilization of the liposomes, leading to rapid clearance of the vesicles from circulation and a burst release of the encapsulated drugs before reaching the target, which may cause undesirable side reactions.[51−53] Therefore, we have pressing need to develop blood stable thermosensitive liposomes.

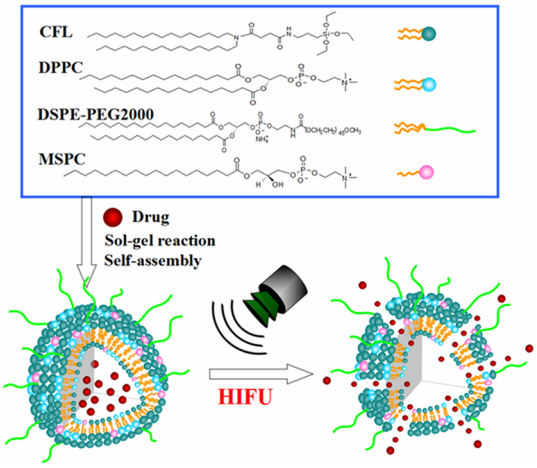


**Figure 1. Schematic illustration for the formation of drug loaded HTSCs and the drug release from HTSCs upon HIFU sonication.**

Recently, a liposomal nanohybrid cerasome has drawn much attention as a new type of drug delivery system since its atomic layer of polyorganosiloxane surface imparts cerasomes higher morphological stability than conventional liposomes while its liposomal bilayer endows better biocompatibility than silica nanoparticles.[54−60] The anticancer drugs loaded cerasomes exhibited sophisticated controlled release behavior and remarkably high stability toward surfactant solubilization, long-term storage, acidic treatment, and all factors that are prone to destabilize conventional liposomes.[54−60] Nevertheless, the drug release from such stable cerasomes is too slow to maintain an effective concentration at the target site, conducing drug resistance in cancer.

With the aim to develop a drug delivery system which is stable enough to minimize drug leakage during blood circulation and mediate a rapid drug release upon HIFU sonication, this study reported the successful fabrication of HIFU and temperature sensitive cerasomes (HTSCs) from a cerasome-froming lipid (CFL) of *N*-[*N*-(3-triethoxysilyl)propylsuccinamoyl]-dihexadecylamine by introducing thermosensitive liposome forming lipids of 1,2-dipalmityol-*sn*-glycero-3-phosphocholine (DPPC), MSPC, and 1,2-distearoyl-*sn*-glycero-3-phosphoethanolamine-*N*-PEG-2000 (DSPE-PEG-2000) into the cerasomes according to the Bangham method in combination of sol−gel reaction and self-assembly process (Figure 1).[54−60] Both hydrophilic and lipophilic chemotherapy drugs were loaded into the internal aqueous core and lipid bilayer of HTSCs, respectively. The physicochemical properties of the HTSCs were characterized and the stability of vesicles was investigated in terms of particle sizes. In addition, the *in vitro* HIFU triggered drug release behavior and *in vivo* antitumor efficacy of the doxorubicin (DOX)-loaded HTSCs were also evaluated.

## RESULTS AND DISCUSSION

**Preparation and Characterization of HTSCs.** As shown in Figure 1, the HIFU and temperature sensitive cerasomes

**TABLE 1. Hydrodynamic Diameter and Zeta Potential of HTSCs with Different Chemical Compositions**

| HTSCs | compositions (molar ratio) CFL:DPPC:MSPC:DSPE-PEG-2000 | hydrodynamic diameter (nm) | zeta potential (mV) |
|---|---|---|---|
| 1 | 25.95%: 60.55%: 9.7%: 3.8% | 178.7 ± 10.1 | −28.6 ± 3.6 |
| 2 | 34.60%: 51.90%: 9.7%: 3.8% | 185.5 ± 9.8 | −30.1 ± 4.2 |
| 3 | 43.25%: 43.25%: 9.7%: 3.8% | 175.3 ± 8.5 | −30.5 ± 5.5 |
| 4 | 51.90%: 34.60%: 9.7%: 3.8% | 186.3 ± 5.5 | −35.8 ± 2.9 |
| 5 | 60.55%: 25.95%: 9.7%: 3.8% | 180.4 ± 10.7 | −38.1 ± 4.5 |

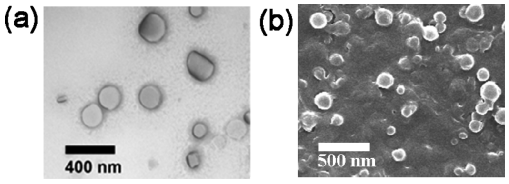


**Figure 2. TEM (a) and SEM (b) images of HTSCs-3.**

of HTSCs are composed of a synergistic combination of four types of lipids including CFL, DPPC, MSPC and DSPE-PEG-2000. Each component could play a different role. CFL acts as the host lipid that forms the bilayer and endows the carrier with high stability. DPPC with a melting transition around 41.5 °C imparts thermal sensitivity to the HTSCs vesicles. MSPC, a mono C18 lipid, can induce thermally enhanced permeability to the encapsulated drugs. DSPE-PEG-2000 is incorporated for long-circulation and ultrafast drug release.[37] In order for modulation of the blood stability and thermal sensitivity of HTSCs, the molar ratios of CFL to DPPC was varied from 25.95% to 60.55% by fixing the contents of MSPC and DSPE-PEG-2000 at 9.7% and 3.8%, respectively.

HTSCs were prepared using a thin-film hydration method in combination of sol−gel reaction and self-assembly process from the mixture of CFL and temperature sensitive lipids (TSL) at different molar ratios (Table 1). Upon ultrasonication, the liposomal bilayer self-assembled and rigidified *via in situ* sol−gel reaction ($Si\text{-}OCH_2CH_3 + H_2O \rightarrow Si{-}OH + CH_3CH_2OH$ followed by $2Si{-}OH \rightarrow Si{-}O{-}Si + H_2O$) on the surface (Figure 1). As shown in Table 1, the mean diameters ($D_{hy}$) of HTSCs were evaluated to be ranging from 170 to 190 nm with narrow particle size distribution by dynamic light scattering (DLS) measurements, well suitable for the application for drug delivery.[58] All these HTSCs were negatively charged and the zeta potentials ranged from −28 to approximately −38 mV due to deprotonation of the silanol groups of CFL on the HTSCs surface, which resembles silica particles. It was found that the zeta potentials of HTSCs increased with the increasing molar ratios of CFL. TEM and SEM images showed that the representative cerasomes of HTSCs-3 were spherical and the vesicular size was consistent with DLS measurements (Figure 2).

Surfactant solubilization method was used to evaluate morphological stability of liposomes in aqueous media. As shown in Figure 3, when nearly 5 equiv of

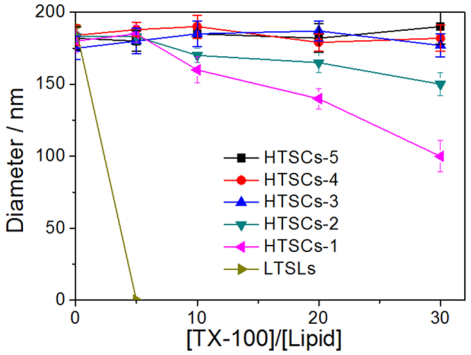


**Figure 3. Hydrodynamic diameters of the various vesicles upon the addition of TX-100 (data represent the mean value for $n = 3$).**

nonionic surfactant Triton X-100 (TX-100) was added to the conventional liposomes of LTSLs consisting of DPPC, MSPC and DSPE-PEG-2000, the hydrodynamic diameter of vesicles drastically decreased, indicating a collapse of the vesicle. On the contrary, the HTSCs exhibited remarkable morphological resistance toward TX-100 because of the formation of siloxane networks surrounding HTSCs surfaces. The DLS analysis revealed little change in the size of HTSCs containing 60.55%, 51.90%, and 43.25% CFL even after up to 30 equiv of TX-100 was added. As the molar ratios of CFL decreased to 25.95% and 34.60%, HTSCs displayed a small reduction in the diameter after the addition of 10 equiv of TX-100. Moreover, the addition of more equivalents of TX-100 resulted in bigger drop in the diameter of HTSCs-1 and HTSCs-2 consisting of 25.95% and 34.60% CFL, respectively. It indicated that HTSCs containing more than 43.25% CFL showed good stability. Nevertheless, the incorporation of more than 43.25% DPPC into HTSCs might block the development of siloxane networks around HTSCs surfaces, conducing to lower stability of the HTSCs.

**Effect of the Vesicular Composition on the Release Behavior of HTSCs.** Three cerasomes (HTSCs-3, HTSCs-4 and HTSCs-5) exhibiting high stability toward surfactant solubilization were then chosen to investigate the effect of the vesicular composition on the release behavior of HTSCs by using calcein as a model drug, a common dye with property of fluorescent quenching at high concentration while dequenching at a low concentration. The *in vitro* calcein release profiles from these stable HTSCs were examined over a time period of experimental observation of 2 min both at 37 and

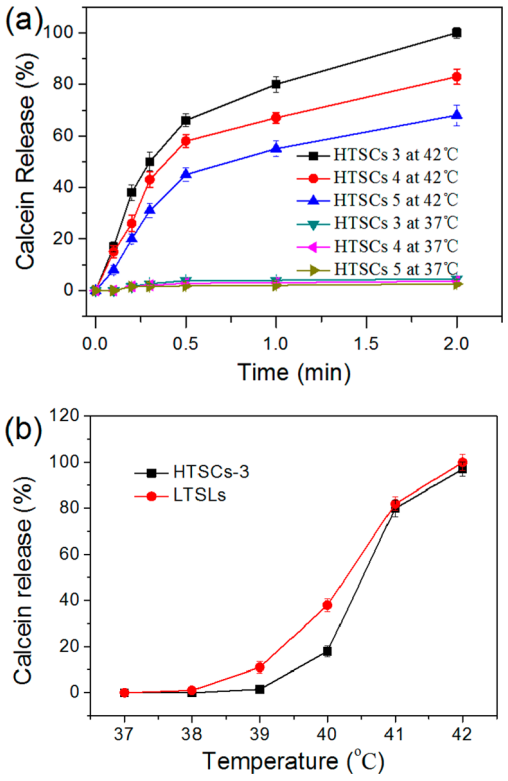


**Figure 4. Effect of the vesicular composition on the release behavior of HTSCs. (a) Calcein release profiles from HTSCs at both 37 and 42 °C. (b) Calcein release from LTSLs and HTSCs-3 in 2 min at different temperatures.**

42 °C (the gel-to-liquid transition temperature of DPPC). As shown in Figure 4a, almost no calcein was released from HTSCs-3, HTSCs-4 and HTSCs-5 at 37 °C and they showed similar release profiles. In contrast, when heated at 42 °C, all these HTSCs vesicles displayed a fast release profiles. HTSCs-3 released nearly 100% calcein within 2 min, while HTSCs-4 and HTSCs-5 released about 83% and 68% of calcein, respectively. Clearly, all three HTSCs were temperature sensitive and the vesicular composition had an obvious effect on the release rate. It is proposed that the presence of MSPC and DSPE-PEG-2000 facilitates rapid release of encapsulated drugs from the HTSCs formulation. The 100 Å toroidal pores formed by lysolipid of MSPC induced permeability of the lipid bilayer membranes.[61] DSPE-PEG-2000 present in the pore, or at the event horizon, provided a steric barrier and repulsive force to stabilize the pore and keep the pore open.[62] In addition, the accumulative release rates of calcein from the composite vesicles decreased as the content of CFL increased. It is attributed to the siloxane networks, which block the drug release channels. Thus, it takes longer time for drugs to be released from HTSCs with the high degree of polymerization.[54] Therefore, HTSCs-3 was selected for further studies due to its good stability and rapid drug release rate.

The temperature responsiveness of HTSCs-3 was evaluated by investigating its drug release profiles over the physiological temperature (37−42 °C) in comparison with conventional LTSLs. As shown in Figure 4b, the release rates increased with increasing temperature for both HTSCs-3 and LTSLs. LTSLs released 11% and 38% of calcein at 39 and 40 °C, respectively, obviously quicker than HTSCs-3. When the temperature increased to above 41 °C, both HTSCs-3 and LTSL displayed a similar release profile and they released near 100% calcein at 42 °C. These results indicated that HTSCs were highly thermosensitive and the optimal temperature for triggering drug release should be 42 °C. In clinical trials, there are still some factors hampering the application of thermosensitive liposomes since mild hyperthermia often cause heterogeneous heat distributions within the tumor tissue due to variations in tumor vascularity, which in turn lead to a variation in drug delivery efficiency.[63] Compared to LTSLs, HTSCs-3 showed a more narrow temperature responsive range, which should be better for heat control to improve the drug release to the full extent in the mild hyperthermia range.

**Biocompatibility of HTSCs.** To maximize chemotherapeutic efficacy on cancer, HTSCs should not only have rapid temperature responsiveness, but also good biocompatibility. Hence, *in vitro* cytotoxicity of HTSCs-3 was first studied by MTT assay by testing the standard cell viability of three kinds of cells including normal cell line of HUVECs cells, immune cells of BMDCs and T cells. As shown in Figure 5A, both HTSCs-3 and LTSLs exhibited low cytotoxicity to HUVECs cells. HUVECs cells remained 90% viable when the HTSCs-3 concentration increases to 0.2 mg/mL. A slight decrease of the cell viability was observed at the HTSCs-3 concentration higher than 0.5 mg/mL, but the HUVECs cell viability was still above 80% when the HTSCs-3 concentration reached 1 mg/mL. This result demonstrated that HTSCs-3 had excellent biocompatibility, which was comparable to traditional liposomes.

BMDC and T cells from SD rats were further used to evaluate the biocompatibility of HTSCs-3. As shown in Figure 5B,C, HTSCs-3 exhibited little cytotoxicity to both BMDC and T cells. Cells viability was then detected by staining with both calcein-AM and propidium iodide (Figures S1 and S2 in Supporting Information). Fluorescence microscopy images showed that the BMDC cells and T cells treated with HTSCs-3 for 48 h exhibited bright green color and no dead cells were observed even at a high concentration of 0.5 mg/mL, consistent with the MTT results. All these data provided an additional evidence that HTSCs-3 had good biocompatibility.

**HIFU Triggered Drug Release Profile of HTSCs.** HIFU sonication induced temperature elevations was first investigated using the duty cycles (DC) of 30% at the working voltage of 180, 185, 190, and 200 mV, respectively. As showed in Figure S3 in the Supporting Information, a thermocouple was fixed in the middle of sample holder to detect the temperature of the

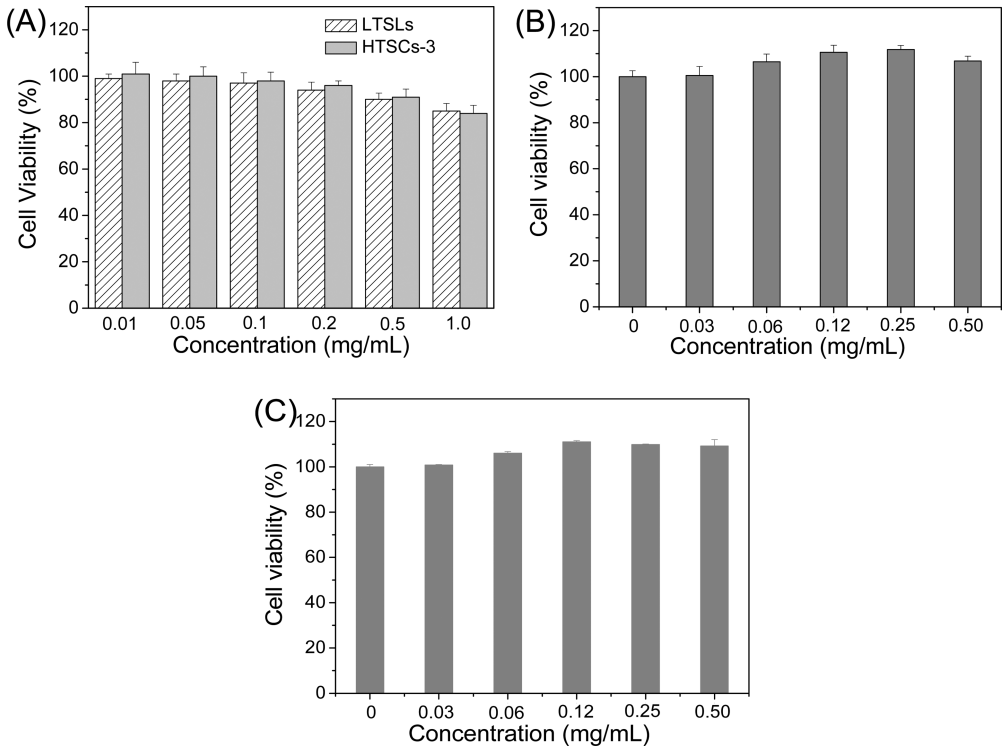


**Figure 5. Biocompatibility of HTSCs-3. (A) Cell viability of HUVECs cells after treatment with different concentrations of HTSCs-3 and LTSLs for 24 h. The cell survival rate of BMDCs cell (B) and T cells (C) after treatment with different concentration of HTSCs-3 for 48 h as determined by MTT assay.**

sample solution under HIFU sonication. The initial temperature was kept at 37 °C by using a water bath. Upon HIFU sonication, the temperature of the sample solution increased to 41 and 43 °C in 175 s when the working voltage was 180 and 200 mV, respectively. Therefore, the working voltage was optimized to be 185−190 mV, where HIFU sonication with the DC of 30% gave a temperature around 42 °C in 175 s (Figure 6).

Numerous studies have demonstrated that HIFU can trigger rapid drug release from thermosensitive liposomes.[42−48] Herein, we investigated the release behavior of both hydrophilic and lipophilic molecules from HTSCs-3 upon HIFU sonication with a working voltage of 190 mV and DC of 30%. As shown in Figure 7a, upon HIFU sonication, the fluorescence intensity of hydrophilic calcein increased gradually with the increasing time, indicating the release of calcein from the HTSCs-3. The HTSCs-3 released 20% calcein in the first 6 s, then 53% calcein in 12 s, and more than 90% calcein released in 1 min (Figure 7b). It indicated that HIFU sonication resulted in much more rapid drug release from HTSCs-3 than heating at 42 °C, where about 80% drug was released from HTSCs-3 in 1 min (Figure 4a). In contrast, without HIFU sonication, the encapsulated calcein was hardly released from HTSCs-3 at all at 37 °C for 8 min. Then, we further investigated the capability of HTSCs-3 to release hydrophobic molecules in PBS solution from their hydrophobic compartment in response to HIFU

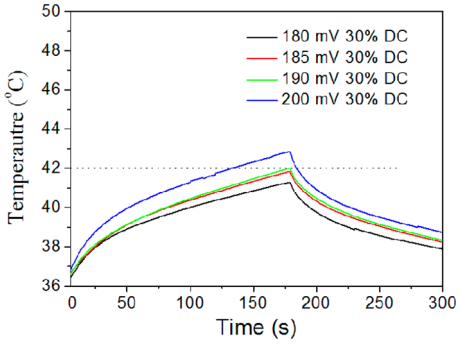


**Figure 6. Optimization of HIFU parameters. Temperature change as a function of time using the duty cycles (DC) of 30% at the working voltage of 180, 185, 190, and 200 mV, respectively. Note that the initial temperature was 37 °C.**

sonication by using lipophilic fluorescent Nile Red (NR) as a model drug. As shown in Figure 7c,d, without HIFU sonication, NR was released very slowly from HTSCs-3 at 37 °C. On the contrary, upon HIFU sonication, the fluorescence intensity of Nile red (NR) decreased gradually with increasing time, suggesting the release of NR from the HTSCs-3 lipid bilayer membrane since the fluorescence intensity of NR is lower in aqueous solution than in the hydrophobic environment of the vesicle membrane.[64] HTSCs-3 released nearly 10% Nile red in the first 2 min, then another 7% NR within the next 6 min. It showed that lipophilic NR had much slower release rate than the hydrophilic calcein, probably due to the strong hydrophobic interaction between NR and the lipid bilayer of HTSCs.[59]

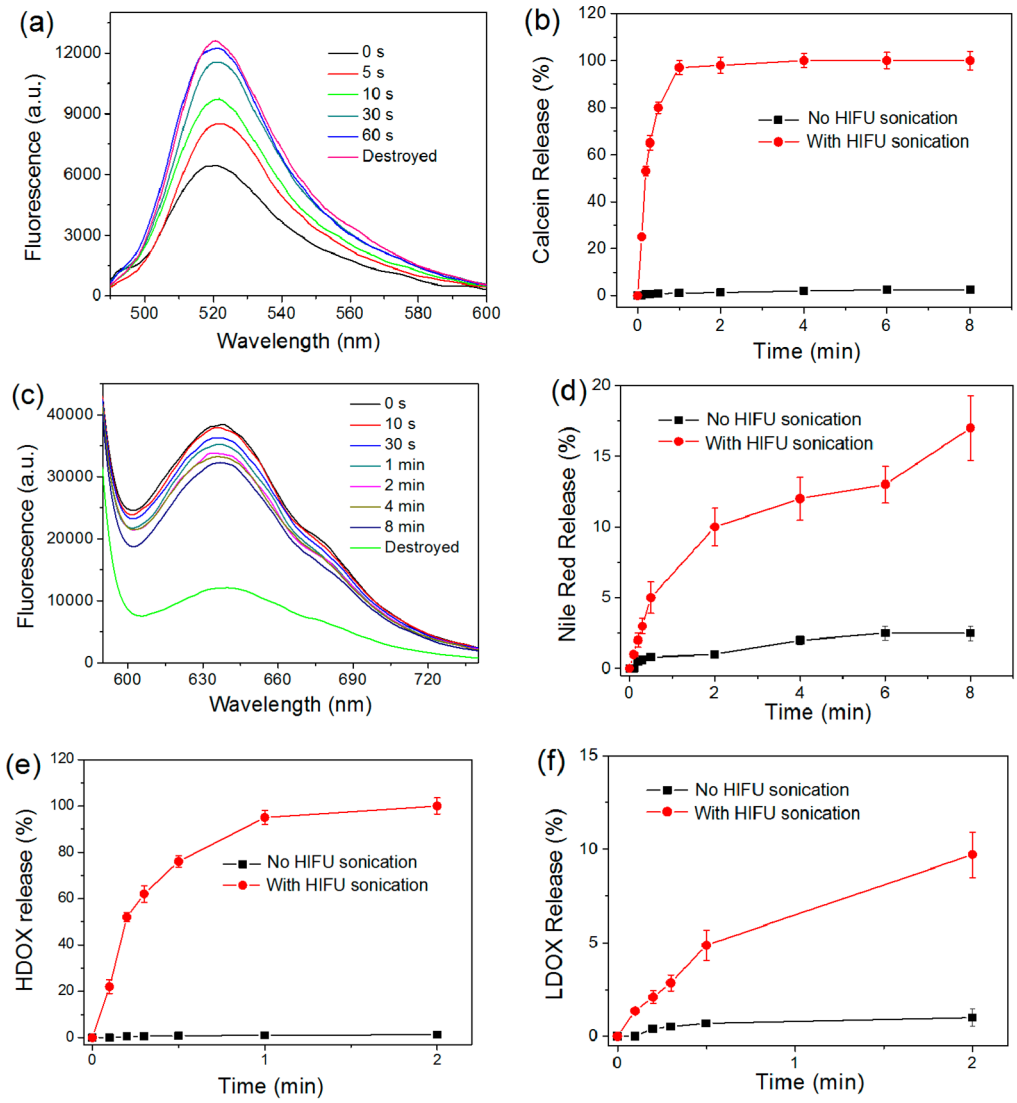


**Figure 7. HIFU triggered drug release profile of HTSCs. (a) Fluorescence spectra of the calcein loaded HTSCs-3; (b) release profile of the calcein loaded HTSCs-3; (c) fluorescence spectra of the Nile red loaded HTSCs-3; (d) Release profile of the Nile red loaded HTSCs-3; (e) release profile of the HDOX loaded HTSCs-3; (f) release profile of the LDOX loaded HTSCs-3 upon HIFU sonication with a working voltage of 190 mV and DC of 30%. Note that the initial temperature was 37 °C in the case of no HIFU sonication.**

Finally, anticancer drugs of hydrophilic doxorubicin hydrochloride (HDOX) and lipophilic doxorubicin (LDOX) were loaded into HTSCs-3 to investigate the HIFU triggered release behavior. Entrapment efficiencies were evaluated to be 58.73 ± 3.20% and 85.51 ± 4.18%, and drug loading contents were 4.06 ± 0.22% and 3.71 ± 0.18% for HDOX-HTSCs-3 and LDOX-HTSCs-3, respectively. Higher encapsulation efficiency (EE) values exhibited by LDOX-HTSCs-3 should be mainly due to the strong hydrophobic interaction between HTSCs lipid bilayer and the lipophilic drug. The zeta potentials were −20.23 ± 0.85 and −30.5 ± 5.51 mV for HDOX-HTSCs-3 and LDOX-HTSCs-3, respectively. HDOX-HTSCs-3 exhibited a higher zeta potential than LDOX-HTSCs-3 due to the protonatable amine residues of some hydrophilic doxorubicin adsorbed on the outer surface of HTSCs-3 *via* electrostatic interaction, thus eliciting an increase of the negative charge.[59] To further evaluate the clinical potential of DOX-HTSCs-3, stability of the HTSCs-3 was tested by measuring DOX leakage as a function of time at 37 °C in serum. We found that both HDOX-HTSCs and LDOX-HTSCs exhibited good stability at 37 °C and released only 9.6 ± 0.9% and 5.5 ± 0.7% encapsulated DOX within 30 min, respectively (Supporting Information Figure S4). In contrast, LTSL showed much lower stability at 37 °C, and 35 ± 1.8% of the encapsulated DOX was leaked after incubation time of 30 min in serum (Supporting Information Figure S4). Due to the minor drug leakage (less than 10% DOX) at physiological temperatures (37 °C), HTSCs-3 showed great potential for *in vivo* drug delivery. Then, HIFU triggering drug release experiment was carried out by using the DOX-loaded HTSCs-3. Similar to the calcein loaded HTSCs-3, almost

no HDOX or LDOX was released from HTSCs-3 at all at 37 °C for 8 min without HIFU sonication. Upon HIFU sonication, the HTSCs-3 released 22% HDOX in the first 6 s, then 52% HDOX in 12 s, and nearly 100% HDOX released in 2 min (Figure 7e). Then, the efficiency of drug release from HTSCs-3 was further assessed in simulated body fluid (SBF) medium which is closer to real biological systems. As shown in Supporting Information Figure S5, HDOX-HTSCs-3 showed similar drug release behavior in both SBF and PBS medium whether HIFU treatment was used or not. The mechanisms for the HIFU triggered rapid drug release from HTSCs-3 may be due to either thermal or nonthermal effects (cavitation and radiation force). The heat induced conformational change of the alkyl chains of the DPPC at 42 °C would lead to an increase in the volume occupied by the hydrocarbon chains in the membrane, while the DSPE-PEG-2000 sensitive to HIFU cavitation would further induced the membrane destabilization,[65] generation of pores on the membranes, and thus an increase in the permeability of the HTSCs bilayer, resulting in ultrafast drug release. Nevertheless, only 9.7% LDOX was released from HTSCs-3 in the first 2 min (Figure 7f), much slower release rate than that for HDOX probably due to the strong hydrophobic interaction between LDOX and the lipid bilayer of HTSCs.[59]

**Pharmacokinetic Profiles of DOX Loaded HTSCs-3.** The blood pharmacokinetics of LDOX-HTSCs-3 and HDOX-HTSCs-3 were monitored in the tumor free mice. The blood samples were collected at 0.2, 0.5, 1, 2, 4, 8, 12, and 24 h after intravenous (iv) injection of the drug loaded HTSCs-3 (Supporting Information Figure S6) followed by the determination of the plasma level of Si and doxorubicin, respectively. The percentage of the injected dose in the blood (ID%) over time was shown in Figure 8. Compared with the pharmacokinetics of DOX in LDOX-HTSCs-3 and HDOX-HTSCs-3, the pharmacokinetics of Si content in LDOX-HTSCs-3 and HDOX-HTSCs-3 displayed a more prolonged blood circulation time and higher blood concentrations, respectively, implying some premature leakage of the encapsulated drugs from the carriers at physiological temperatures (37 °C) followed by a rapid blood clearance of the leaky drugs. In addition, HDOX-HTSCs-3 exhibited higher drug release rate than the LDOX-HTSCs-3, consistent with the *in vitro* drug release experiments (Supporting Information Figure S4). Approximately 81.7 ± 7.1% and 79.3 ± 6.3% of DOX remained in the blood circulation at 30 min after the administration of LDOX-HTSCs-3 and HDOX-HTSCs-3, and 71.8 ± 6.7% and 63.4 ± 5.5% remained after 1 h. This can easily be explained by the increase in hydrophobic interaction between the HTSCs bilayer and LDOX. Moreover, HDOX-HTSCs-3 showed slightly slower blood clearance than LDOX-HTSCs-3, which might be due to the lower negative charge of HDOX-HTSCs-3 (~ −20.2 mV). LDOX-HTSCs-3 (~ −30.5 mV) with higher

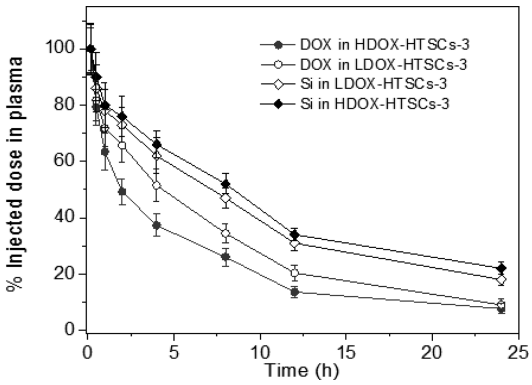


**Figure 8. Pharmacokinetics profiles of the drug loaded HTSCs-3, which were monitored by determining the plasma level of Si in HDOX-HTSCs-3 (closed squares) and LDOX-HTSCs-3 (open squares), as well as the plasma level of DOX in HDOX-HTSCs-3 (closed circles) and LDOX-HTSCs-3 (open circles), respectively. Data are mean ± SD ($n$ = 5).**

charge density were more easily taken up by reticuloendothelial system (RES), resulting in relatively shorter half-life.[66−68] The area under the plasma concentration−time curve (AUC) was calculated for 0−24 h, showing the order of Si in HDOX-HTSCs-3 (1047.7 ± 85.1%ID·h) > Si in LDOX-HTSCs-3 (955.5 ± 56.4%ID·h) > DOX in LDOX-HTSCs-3 (718.2 ± 84.8%ID·h) > DOX in HDOX-HTSCs-3 (547.7 ± 71.5%ID·h). The half-life time ($t_{1/2}$) was evaluated to be 12.3 ± 0.95 h for Si in HDOX-HTSCs-3, 10.9 ± 1.12 h for Si in LDOX-HTSCs-3, 8.50 ± 1.49 h for DOX in LDOX-HTSCs-3, and 8.87 ± 1.79 h for DOX in HDOX-HTSCs-3. Although there was some premature drug release of HTSCs-3, the HDOX and LDOX in DOX loaded HTSCs-3 still showed remarkably higher half-life (8.87 ± 1.79 and 8.50 ± 1.49 h) than the reported conventional LTSL (0.92 ± 0.17 h).[48] All these data demonstrated that HTSCs-3 had high blood stability and the DOX loaded HTSCs-3 displayed a significantly long blood circulation time, which were very suitable for *in vivo* drug delivery.

**Biodistribution Study of DOX Loaded HTSCs-3 under Mild Hyperthermia Using HIFU.** The *in vivo* biodistribution of the drug loaded HTSCs was studied in BALB/c mice bearing two tumors at both lower legs of BALB/c mice. The tumor on the right leg was used as the untreated control and the tumor on the left leg was treated with HIFU immediately after the iv injection of 5 mg DOX/kg HDOX-HTSCs-3 and LDOX-HTSCs-3, respectively. Then, the DOX content in the tissues was determined along with the measurement of Si content in the tissues (Figure 9). The measurements of both DOX and Si content in tissues showed that HIFU treatment led to significantly increased tumor uptake of HDOX-HTSCs-3 and LDOX-HTSCs-3 as compared to the untreated tumor. In addition, the DOX content was much higher than the corresponding Si content at the treated tumor tissue. These results were expected since HIFU treatment can not only enhanced the DOX loaded HTSCs-3 uptake, but also triggering the DOX release from their

carrier of HTSCs-3 when circulating through the tumor site. The DOX uptake in the HIFU treated tumor increased by 3.5-fold and 2.7-fold compared to the non-HIFU treated one for HDOX-HTSCs-3 and LDOX-HTSCs-3, respectively. Moreover, HDOX-HTSCs-3 enhanced the delivery of DOX to the HIFU-treated tumor by 1.72-fold compared to LDOX-HTSCs-3.

It was noteworthy that in most organs including untreated tumor, heart, spleen, and kidney, the magnitude of organ uptake for HDOX-HTSCs-3 was slightly higher than that for LDOX-HTSCs-3. In contrast, LDOX-HTSCs-3 showed significantly higher uptake in the liver than the HDOX-HTSCs-3 (Figure 9). This may be due to the surface charge difference between HDOX-HTSCs-3 and LDOX-HTSCs-3. LDOX-HTSCs-3 ($\sim -30.5$ mV) with higher charge density may cause higher liver uptake than less negatively charged HDOX-HTSCs-3 ($\sim -20.2$ mV), which was likely due to active phagocytosis by macrophages (Kupffer cells) in the liver.[68−71] The relative lower uptake of less negatively charged HDOX-HTSCs-3 in the liver may be attributed to the electrostatic repulsion that minimize the recognition and nonspecific uptake by macrophages in the liver.[71,72] Furthermore, it can be found that the content of doxorubicin in most organs was lower than the amount of Si except for the treated tumor and kidney. This can be caused by the uptake of DOX-HTSCs-3 that already lost part of their DOX contents during the circulation and HIFU treatment.

**Antitumor Efficacy of DOX Loaded HTSCs-3 under Mild Hyperthermia Using HIFU.** The rapid temperature responsiveness and good blood stability of HTSCs-3 encouraged us to investigate the *in vivo* therapeutic efficacy of the DOX loaded HTSCs-3. Female BALB/c mice bearing MDA-MB-231 tumor were divided into 6 groups with 8 mice in each group: PBS only, HDOX-HTSCs-3 only, LDOX-HTSCs-3 only, PBS + HIFU, HDOX-HTSCs-3 + HIFU, and LDOX-HTSCs-3 + HIFU. The drug loaded HTSCs-3 suspensions in PBS were intravenously injected into the mice (dose: 5 mg DOX $kg^{-1}$). Then, the tumor areas of the mice in the three HIFU groups with continuous anesthesia were exposed to pulsed-HIFU sonication at DC of 30% and voltage of 190 mV for 5 min twice: immediately and 24 h after injection. The tumor temperature change was monitored during HIFU sonication. The temperature in the tumor areas of mice from the HDOX-HTSCs-3 + HIFU group rapidly increased to about 42 °C within 100 s, and maintained at this temperature for nearly 200 s, which was long enough to release the drug from the carriers of HTSCs-3 in the tumor. Similar result was also observed for the LDOX-HTSCs-3 + HIFU and PBS + HIFU groups (Figure 10A). In contrast, the control group without HIFU sonication maintained the temperature at about 37 °C.

The therapeutic effectiveness was evaluated by measuring the tumor sizes and the representative mice photographs of each group were recorded at certain

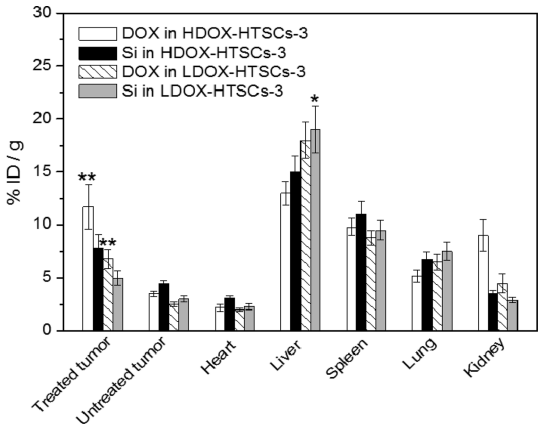


**Figure 9. Biodistribution of DOX and Si element at 1 h after the iv injection of 5 mg DOX/kg HDOX-HTSCs-3 and LDOX-HTSCs-3 in combination with local HIFU treatment to the tumor in the left lower leg. The tumor in the right leg served as the untreated control. Data are mean ± SD ($n = 5$). **$p < 0.01$, significant difference compared with the untreated tumor; *$p < 0.05$, significant difference compared with HDOX-HTSCs-3 in liver.**

day after treatment (Figure 10B−F). We found that inoculated tumors grew uniformly over time in the groups of PBS only and PBS + HIFU, showing similar tumor growth rate; tumor volume increased from ~106 to approximately 240 $mm^3$ at 16 days after treatment (Figure 10B and Figure S7 in Supporting Information). These results indicated that HIFU sonication alone at the experimental condition did not cause potential destructive effects; the absence of any harmful effects was not surprising in light of the low mean peak temperatures elevations of 4−5 °C measured in the tumors during the exposures. In contrast, the tumors were effectively inhibited in both HDOX-HTSCs-3 only and LDOX-HTSCs-3 only groups (Figure 10B−D). At 16 day after treatment, the tumor volume of the LDOX-HTSCs-3 only group was maintained at about 127 $mm^3$ while reducing to 71 $mm^3$ for the HDOX-HTSCs-3 only group. The therapeutic difference between these two groups maybe due to the slower drug release rate of LDOX-HTSCs-3. The above results revealed that the DOX loaded HTSCs-3 could accumulate in the tumor tissue and perform a sustained release of the encapsulated drug in the acidic tumor environment to inhibit the tumor growth. As expected, excellent therapeutic effectiveness was clearly observed for the HDOX-HTSCs-3 + HIFU and LDOX-HTSCs-3 + HIFU groups, and tumors were further effectively destroyed as compared to the drug groups without HIFU sonication, leaving scars at their original sites which fell off after about 16 days (Figure 10E,F). This could be explained by the fact that upon HIFU sonication immediately after DOX-HTSCs-3 administration, HTSCs released partial drugs quickly when they circulated through the blood vessels at the tumor site,[29] inducing local high concentration of drugs in the tumor. Another HIFU treatment at 24 h

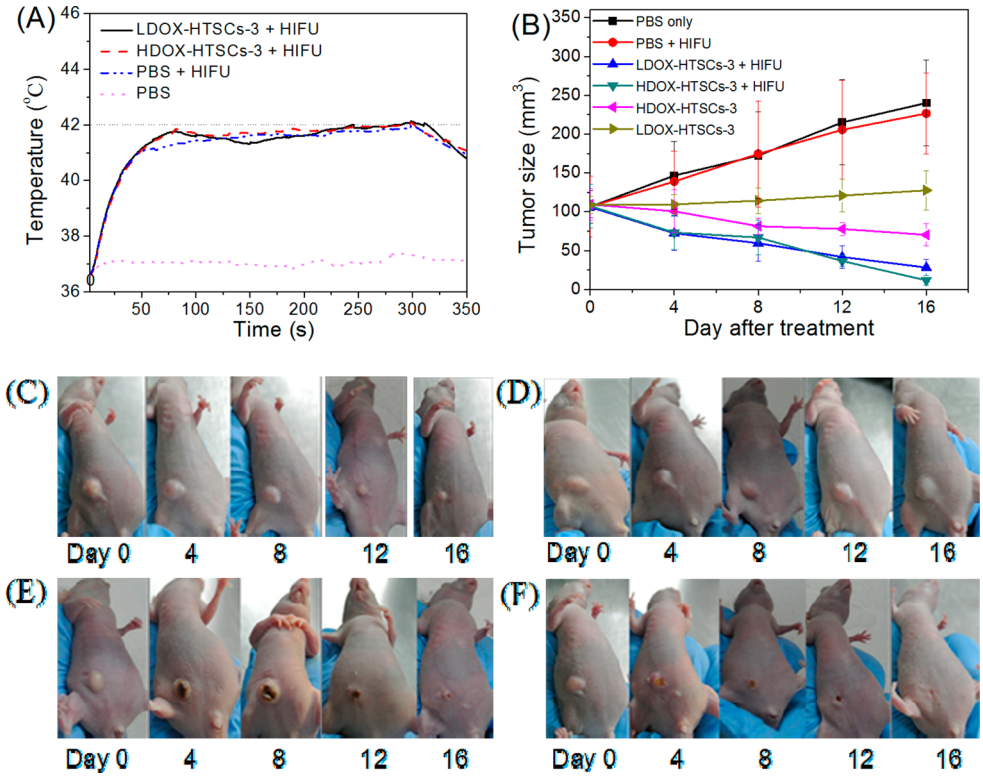


**Figure 10. Antitumor efficacy using HIFU. (A) Temperature change curves of the nude mice tumor after different treatments as a function of HIFU exposure time with working voltage of 190 mV and DC of 30%. (B) Tumor volume change with time after different treatments. Representative photographs of tumor-bearing mice before and after various treatments for 4, 8, 12, and 16 days: (C) HDOX-HTSCs-3 only; (D) LDOX-HTSCs-3 only; (E) HDOX-HTSCs-3 and HIFU sonication; (F) LDOX-HTSCs-3 and HIFU sonication.**

after injection further triggered drug release from HTSCs-3 accumulated in the tumor area by the EPR effect, resulting in more effective tumor drug concentration, especially for the LDOX-HTSCs-3 treated group. Although drug release rate of LDOX-HTSCs-3 under HIFU sonication was obviously slower than that of HDOX-HTSCs-3, double HIFU sonication could induce sufficient therapeutic drug concentration in the tumor, resulting in similar therapeutic efficacy of the two groups. Compared with the other groups, the two DOX-HTSCs-3 + HIFU groups exhibited much higher anticancer efficacy. This is because the HTSCs formulation was stable enough to retain drug molecules inside the vesicles and to be delivered to the tumor by EPR effect during blood circulation, as well as thermosensitive enough to give a rapid drug release over physiological temperature (39−42 °C) upon HIFU sonication. In addition, HIFU may improve the transcapillary transport, improve the transport through the extracellular matrix, and facilitate the cellular uptake. It has been reported that silica nanoparticles could be used as sensitizing agents for HIFU therapy.[73,74] HTSCs with a partial silica surface combined some characteristics of both silica and liposome, so it is quite valuable to evaluate the potential of HTSCs to assist HIFU therapy. It is known that the conventional LTSLs still shows some limitations in antitumor efficacy study due to its relatively short half-life and the drug leakage during blood circulation. On the contrary, HTSCs-3 showed significantly higher stability and longer blood circulation time than LTSLs, beneficial for maximizing the effect of chemotherapy on cancer. On the other hand, longer lag time between intravenous injection and HIFU treatment would facilitate practical operation in clinical application; thus, the therapeutic effect of HTSCs + HIFU (24 h) treatment groups was worth further systematic investigation. For assessing the *in vivo* toxicity of drug loaded HTSCs-3 to healthy tissue, the vital organs including heart, liver, spleen, lung, and kidney of the HDOX-HTSCs-3 and LDOX-HTSCs-3 treated mice without HIFU treatments were collected at 16 days after treatment and used for further histological examination. Hematoxylin and eosin (H&E) stained images showed that neither noticeable organ damage nor inflammation could be observed in all major organs of the treated mice (Supporting Information Figure S8), indicating the relative lower accumulation and slower release rate in the normal tissues because of the high stability of drug loaded HTSCs-3 with longer blood circulation time. Change of mice body weight was also investigated, as shown in Figure S9 in the Supporting Information. No apparent difference was observed among different groups within 16 days, suggesting that all

treatments were tolerated well by the tumor-bearing mice. Therefore, the drug loaded HTSCs-3 in combination with HIFU sonication could be used as a powerful therapeutic strategy for *in vivo* treatment of cancer. Furthermore, the HTSCs may be exploited to load antimicrobial agents or even antifever drugs like aspirin or paracetamol, which can be released during high fever (above 42 °C). Obviously in this case, there is no need for ultrasound; HTSCs can make smart drug release according to the circumstances of the cell.[75]

## CONCLUSIONS

We reported the successful fabrication of the temperature-sensitive nanohybrid cerasomes of HTSCs with high physiological stability and tunable release characteristics by introducing LTSLs lipid components into cerasomes. The HTSCs had a blood circulation time with half-life >8.50 ± 1.49 h, much longer than conventional LTSLs (0.92 ± 0.17 h). Such high blood stability can avoid rapid clearance of the vesicles from circulation and a burst release of the encapsulated drugs before reaching the target which may cause undesirable side reactions. In addition, the introduced LTSLs lipid components can change structure quickly at an elevated temperature generated by HIFU exposure, creating channels in the liposome bilayer that guarantee the drug release mainly occurring within the designated area in need of treatment. We found that the HTSCs could released more than 90% hydrophilic drugs in 1 min upon HIFU sonication. The *in vivo* experiments showed that the tumor growth was significantly suppressed after systemic administration of drug loaded HTSCs, followed by double HIFU sonication. As a result, HTSCs in combination with HIFU not only enable the delivery of higher concentrations of chemotherapy drugs directly to the tumor and achieve maximum therapeutic efficacy and minimal side effects, but also avoid the damage to the healthy tissues caused by systemic administration of drugs. Therefore, HTSCs combined with HIFU hold great potential for efficient local chemotherapy of cancer. The HTSCs platform also has the capability to be employed on a variety of drug products. In addition, there is still room for improvement of HTSCs. The new lipids and membrane compositions reported by May *et al.*[63] could be considered to combine with cerasomes to further modulate HTSCs thermosensitivity. For enhancing release of hydrophobic drugs, the combination of cerasome with gas generating agents such as perfluoropentane[76] and ammonium bicarbonate[77] may be a good choice. The generated gas bubbles may induce permeable defects in the lipid bilayer that could rapidly trigger local drug release upon heating, the investigation of which is under way in our laboratory.

## MATERIAL AND METHODS

**Lipids and Chemical Reagents.** All chemicals and lipids were commercially available and used as obtained. Cerasome forming lipid of *N*-[*N*-(3-triethoxysilyl)propylsuccinamoyl]-dihexadecylamine was synthesized according to the reported method.[54−60] DPPC, DSPC, and DSPE-PEG-2000 were provided by Lipoid (Ludwigshafen, Germany). MSPC was purchased from Avanti Polar Lipid, Inc. HDOX was purchased from Pharmachemie, and LDOX was obtained by treating HDOX with triethylamine according to the report methods.[78] Calcein and NR were supplied by Sigma-Aldrich (Steinheim, Germany). Deionized water (DI water) (resistivity 18.2 MΩ·cm$^{-2}$) was obtained by purification of house-distilled water with a Milli-Q Gradient System, and simulated body fluid (SBF) were prepared according to the literature.[79]

**Preparation of HIFU and Temperature Sensitive Cerasomes.** Unloaded HTSCs were prepared using the conventional Bangham method, in combination with a sol−gel method and self-assembly process.[54−60] Briefly, the lipid materials including CFL, DPPC, MSPC and DSPE-PEG-2000 at various molar ratios were codissolved in chloroform. After removal of the organic solvent in a vacuum rotary evaporator, the resulted lipid thin film was then dried overnight in vacuum and hydrated in DI water at 45 °C for about 30 min followed by vortex for 20 min. The obtained suspensions of multilamellar vesicles were further ultrasonicated with a probe-type sonicator for 3 min in an ice bath. Conventional low temperature sensitive liposomes (LTSLs) consisting of DPPC, MSPC, and DSPE-PEG-2000 (the molar percentage ratio is 86.5:9.7:3.8) were prepared using the same procedure.

Calcein-loaded HTSCs (Calcein-HTSCs), NR-loaded HTSCs (NR-HTSCs), hydrophilic DOX-loaded HTSCs (HDOX-HTSCs), hydrophilic DOX-loaded LTSLs (HDOX-LTSLs) and lipophilic DOX-loaded HTSC (LDOX-HTSCs) were also prepared as described above. For DOX loading, the used molar ratios of drug to total lipids were 1:30 for LDOX or 1:10 for HDOX according to the reported methods.[57−59] The unentrapped NR and LDOX were separated by centrifugation at 6000 rpm for 10 min, and the unloaded calcein and HDOX were removed by passing through a sephadex G-50 column with PBS as an eluent. All samples were stored at 4 °C in a sealed container for further studies. The whole procedure was performed in the dark.

**HTSCs Characterization.** The size distribution and zeta potential of the blank and drug-loaded HTSCs were determined using a 90Plus/BI-MAS dynamic light scattering (DLS) analyzer (Brookhaven Instruments Co.). Vesicle suspensions were diluted with PBS before the measurement. Six replicate measurements were performed using a wavelength of 632.8 nm at a scattering angle of 90° at room temperature. The obtained data were analyzed in automatic mode. Vesicle size is expressed as intensity mean diameter ± SD of values.

The morphology and structure of HTSCs were analyzed by scanning electron microscopy (SEM) and transmission electron microscopy (TEM). The SEM specimens were prepared by casting an aliquot of the HTSCs suspension onto copper foil. The specimens were sputtered with gold for 2 min, and then inspected using a Hitachi S-4800 field emission scanning electron microscope. TEM evaluation was carried out using an H-7650 apparatus (Tokyo, Japan) with a tungsten filament at an accelerating voltage of 100 kV. Briefly, the TEM sample was prepared by depositing the particle suspension (200 mmol/mL) onto a 300-mesh Formvar-coated copper grid. Samples were blotted away after 10 min incubation, and the grids were negatively stained with freshly prepared and sterile filtered 2 wt % uranyl acetate aqueous solution for 5 min at room temperature. The grids were then washed twice with distilled water and air-dried prior to imaging.

**Evaluation of Drug Loading Content and Encapsulation Efficiency.** The amount of DOX entrapped in the HTSCs was measured spectrophotometrically.[57] Specifically, 0.5 mL of HTSCs (40 μM) was suspended in 0.5 mL of HCl solution (1 M), followed vigorous

stirring overnight and centrifugation at 6000 rpm for 10 min. The fluorescence intensity of the DOX solutions was measured at an excitation wavelength of 480 nm and an emission wavelength of 580 nm. The amount of DOX was determined by fluorescence spectrophotometry using the corresponding standard calibration curve, and the weight of the vesicles was determined after freeze-drying. The encapsulation efficiency (EE) and drug loading content (DLC) were calculated as

$$\mathrm{EE}(\%) = \frac{\text{Weight of drug encapsulated in HTSCs}}{\text{Initial weight of drug}} \times 100$$

$$\mathrm{DLC}(\%) = \frac{\text{Weight of drug in HTSCs}}{\text{Total weight of drug and lipid}} \times 100$$

**Cell Culture and Biocompatibility Study of HTSCs.** Human umbilical vein endothelial cells (HUVECs) were cultured in RPMI-1640 medium supplemented with 2 $mmol \cdot L^{-1}$ L-glutamine, 500 $U \cdot mL^{-1}$ penicillin, 10% fetal bovine serum (FBS), and 50 $\mu g \cdot mL^{-1}$ streptomycin at 37 °C in a humidified atmosphere containing 5% $CO_2$. Bone marrow dendritic cells (BMDC) were generated by culturing bone marrow stem cells from SD rats in complete IMDM (Iscove's Modified Dulbecco's Medium) with 20 $ng \cdot mL^{-1}$ recombinant granulocyte/macrophage colony stimulating for 6 days at 37 °C and T cells obtained from SD rats were cultured in cIMDM at 37 °C. Biocompatibility of the HTSCs to HUVECs was investigated by the MTT assay. Briefly, HUVECs cells were plated at a density of $1 \times 10^5$ cells/well in 96-well plates at 37 °C in 5% $CO_2$ atmosphere. Wells without cells acted as blank control. After 24 h, the medium was replaced with fresh medium containing blank HTSCs at the final concentrations of 0.01, 0.05, 0.1, 0.2, 0.5, and 1.0 $mg \cdot mL^{-1}$. Every concentration was added to five wells as parallel control and wells without HTSCs as negative control. After 24 h, 20 $\mu$L of MTT at a concentration of 5 $mg \cdot mL^{-1}$ was added to each well and the samples were incubated for 4 h. Then, the medium was removed and 150 $\mu$L of DMSO was added. The absorbance of each well was recorded at 560 nm with a microplate reader (Multidkan MK3, Thermo). Five replicate wells were run for each concentration and each experiment was repeated three times. BMDC cells and T cells were also used for evaluation according to the same procedure as descried above. After incubation with HTSCs for 48 h, cell viability was further determined by staining with both calcein-AM and PI, and observed using a fluorescence microscope.

**Pharmacokinetic Study of Drug Loaded HTSCs.** Wistar rats were obtained from Vital River, Beijing. To determine the circulation time, HDOX-HTSCs and LDOX-HTSCs (5 mg of DOX/kg) were injected into tumor free rats *via* the tail vein. Blood samples (0.3 mL) were collected at the time points of 0.2, 0.5, 1, 2, 4, 8, 12, and 24 h after intravenous injection. The pharmacokinetics profile of HTSCs in bloodstream was finally evaluated by measuring the Si content in blood over the course of 24 h *via* Inductively Coupled Plasma (ICP) method after decomposing the blood samples by *aqua regia*. The DOX content in the plasma was measured according to reported methods.[48] Briefly, the blood was first collected in a tube and centrifuged at 2500 rpm at 4 °C for 15 min to isolated the plasma, then mixing 10 $\mu$L of plasma with 990 $\mu$L of acidified isopropyl alcohol, and the resulting mixture was incubated at 4 °C in the dark overnight. Finally, the resulting sample was centrifuged for 10 min at 12 000*g* and the supernatant was transferred into a 96-well plate for determination of fluorescence at the excitation wavelength of 480 nm and the emission wavelength of 580 nm. The plasma DOX concentration was determined by comparing the fluorescence with a calibration curve generated from known amounts of DOX in mouse plasma. Parameters including elimination half-life ($T_{1/2}$) and area under the plasma concentration–time curve from zero to time infinity (AUC) were evaluated by using the Kinetica software package (version 5.0, Thermo Fisher Scientific Inc., MA). All the animal experiments were approved by institutional animal use committee and carried out ethically and humanely.

**Biodistribution Study.** The experiment was performed according to the reported method.[48] The MDA-MB-231 cells ($\sim 5 \times 10^7$ cells) were subcutaneously implanted into both lower legs of female BALB/c athymic nude mice. When the tumors volume reached $\sim$106 $mm^3$, the mice were anesthetized, and the left lower leg was immersed into a water bath maintained at 37 °C. The tumor was then treated with HIFU for 5 min immediately after the iv injection of different drug formulations (5 mg DOX/kg). The tumor on the right leg was used as the untreated control. One hour after the treatment, the mice were sacrificed, and major organs including tumors, heart, liver, spleen, lung and kidney were excised. The tissue samples were washed with PBS and weighed after removing excess fluid. The Si content in the tissues was assessed *via* ICP measurement after decomposing the tissue samples by *aqua regia*. The DOX content in the tissues was determined using the method described previously.[48] Briefly, tissue samples (about 100 mg) were first suspended in 1.5 mL of nuclear lysis buffer (10 mM HEPES, 1 mM $MgSO_4$, 1 mM $CaCl_2$, pH 7.4) and homogenized by a tissue homogenizer ($2 \times 30$ s at 6600 rpm). An aliquot of the homogenate (100 $\mu$L) was transferred into a 1.5 mL microtube, and then a mixture consisting of 50 $\mu$L of 10% (v/v) Triton X-100, 100 $\mu$L of water, and 750 $\mu$L of acidified isopropyl alcohol was added and the resulting mixture was stored at −20 °C overnight. Then, the mixture was thawed and centrifuged for 10 min at 12 000*g*, and the supernatant was transferred into a 96-well plate (Ex 480 nm/Em 580 nm) for DOX determination. The data were compared with standard curves made from spiking known amounts of DOX into different tissue homogenates from the untreated mice to get the absolute quantification of DOX in different tissues.

**HIFU Equipment Used for *in Vitro* Drug Release.** The HIFU equipment employed in this research was made in-house. It comprises two main components: ultrasound generator and acoustic lens transducer. The schematic diagram of apparatus is shown in Figure S3 in Supporting Information. The acoustic lens transducer with an effective diameter of 64 mm and a focal length of 52 mm was mounted at the bottom of a tank filled with water (37 °C, mimicking the *in vivo* situation) and the beams of ultrasound were pointed upward and focused as a circular spot. The ultrasound output power can be adjusted in the range of 0–100 W and the frequency of ultrasound is 0.5 MHz. The focused beams of ultrasound passed through latex membrane and acted on the sample solution in the cuvette reactor. The water bath was covered by ultrasound-absorbing material to avoid ultrasound reflection before HIFU exposure. The temperature at the position of the focal point was measured with a thermocouple fixed in the middle of sample holder.

**The Drug Release Behavior of HTSCs Triggered by Heat and HIFU.** The drug release behavior of HTSCs triggered by heat and HIFU was investigated using the reported method.[37] Briefly, calcein release was determined using a fluorescence dequenching assay. For heat triggered release, 1 mL of different calcein-loaded HTSCs was added to 30 mL of PBS preheated to 37, 38, 39, 40, 41, 42 °C using a thermostat-controlled water bath and mixed well. At certain time intervals, 2 mL samples were taken and cooled on ice to quickly stop drug release. For HIFU triggered release, 1 mL of calcein loaded HTSCs was added to 30 mL of PBS preheated to 37 °C and mixed well, then 2 mL of the sample was added to the cuvette reactor (Figure S3 in Supporting Information), and HIFU sonication was performed. At certain time intervals, samples were taken and cooled on ice to quickly stop drug release. The percentage of the released calcein was calculated by

$$\text{Release Efficiency}(\%) = \frac{F(t) - F_0}{F_c - F_0} \times 100\%$$

where $F(t)$ is the fluorescence of the sample treated by heat or HIFU followed by cooling down on ice and equilibrating back to room temperature, $F_0$ is the florescence of the control sample with no heat or HIFU treatment, and $F_c$ is the average fluorescence of six of the samples after being destroyed. The calcein in each sample was quantified separately by fluorescence in a Thermo Scientific Lumina spectrofluorophotometer using an excitation wavelength of 490 nm and an emission wavelength of 520 nm. The release of both DOX and NR in PBS, SBF, or serum from the HTSCs or LTSLs was performed and calculated similarly

as described for calcein release. The used excitation and emission wavelengths were 480 and 580 nm for the DOX release and 570 and 630 nm for the NR release, respectively. All experiments were performed in triplicate.

**Antitumor Efficacy Study of the HDOX-HTSCs and LDOX-HTSCs.** *Mice and Tumors.* All animal work was done according to an approved animal protocol and in strict compliance with the Animal Care and Use Committee guidelines and regulations of Institutional Animal Care and Use Committee at the Institute of Biophysics of Peking University. A mammary adenocarcinoma cell line of MDA-MB-231 was selected. The cells were cultured in RPMI 1640 with 10% fetal bovine serum, supplemented with L-glutamine (200 mmol/L) and 2.2% of 100× penicillin−streptomycin, and incubated at 37 °C and 5% $CO_2$. For tumor inoculations, female BALB/c athymic nude mice (5−6 weeks old) were implanted by a subcutaneous injection of $\sim 5 \times 10^7$ cells in PBS at the right abdominal mammary position.

*Pulsed-HIFU Exposures.* All mice were anesthetized with inhalation isoflurane throughout the pulsed-HIFU exposure process. Each mouse was positioned in a holder, and tumor was placed upon the hole of the holder in a tank of degassed water maintained at 37 °C. This positioning allowed for the entire tumor to be treated directly within the focal zone of the transducer. The used exposure parameters were 190 mV of voltage, 5 kHz of pulse repetition frequency, and 30% duty cycle (DC) (30 ms ON/70 ms OFF).

*Tumor Temperature Detection under HIFU Sonication.* Briefly, during the whole HIFU exposure process, the temperature inside tumors was measured with a thermometer with super miniature type temperature probe (diameter = 0.5 $\mu$m, Guang Zhou Sungun Measurement and Control Technology Co., Ltd.), in which one thermocouple was placed in the tumor without HIFU sonication served as an external control, a second thermocouple was placed in the tumor outside of the region being exposed to HIFU. The profile showed an exponential increase in temperature and then stabilization of the peak temperature during the exposure, followed by an exponential thermal relaxation to baseline.

*Effects on Tumor Growth.* In this experiment, tumors were grown at the right abdominal mammary position. Treatments were started when the tumors volume reached $\sim$106 $mm^3$, which was designated as day 0. The tumor-bearing mice were divided into 6 groups with 8 mice in each group: PBS only group, HDOX-HTSCs-3 only group, LDOX-HTSCs-3 only group, PBS + HIFU group, HDOX-HTSCs-3 + HIFU group, and LDOX-HTSCs-3 + HIFU group. A volume of 200 $\mu$L (dose: 5 mg DOX/kg) HDOX-HTSCs-3 or LDOX-HTSCs-3 was intravenously (iv) injected into the tumor-bearing mice, and treated with pulsed-HIFU at 190 mV with DC of 30% for 5 min. Double pulsed-HIFU exposures were given immediately following the injections and 24 h later. The tumor sizes were measured by a caliper at certain time interval; tumor volume was calculated as $V = (L \times W^2)/2$, where $L$ and $W$ were the length and width of the tumor, respectively. In addition, mice were sacrificed after 16 days, and major organs including heart, liver, spleen, lung, and kidney were collected and fixed in formalin. Fixed tissue specimens were embedded in paraffin, stained with hematoxylin and eosin (H&E), and subsequently examined by light-field microscopy.

**Statistical Analysis.** Results are presented as mean ± SD. The mean *in vivo* drug and silicon contents difference in major organs among different groups was analyzed by the Student's $t$ test, with $p < 0.05$ considered to be statistically significant.

*Conflict of Interest:* The authors declare no competing financial interest.

*Acknowledgment.* This work was financially supported by State Key Program of National Natural Science of China (Grant No. 81230036), National Natural Science Foundation of China (No. 21273014 and No. 81201186), National Natural Science Foundation for Distinguished Young Scholars (No. 81225011) and China Postdoctoral Science Foundation (2013M530014).

*Supporting Information Available:* Other experimental details, additional figures and characterization data. This material is available free of charge *via* the Internet at http://pubs.acs.org.

## REFERENCES AND NOTES

1. Singal, P. K.; Iliskovic, N. Doxorubicin-Induced Cardiomyopathy. *N. Engl. J. Med.* **1998**, *339*, 900–905.
2. Slamon, D. J.; Leyland-Jones, B.; Shak, S.; Fuchs, H.; Paton, V.; Bajamonde, A.; Fleming, T.; Eiermann, W.; Wolter, J.; Pegram, M.; et al. Use of Chemotherapy Plus Amonoclonal Antibody Against HER2 Formetastatic Breast Cancer that Overexpresses HER2. *N. Engl. J. Med.* **2001**, *344*, 783–792.
3. Kessler, D. A.; Austin, R. H.; Levine, H. Resistance to Chemotherapy: Patient Variability and Cellular Heterogeneity. *Cancer Res.* **2014**, *74*, 4663–4670.
4. Moitra, K.; Lou, H.; Dean, M. Multidrug Efflux Pumps and Cancer Stem Cells: Insights into Multidrug Resistance and Therapeutic Development. *Clin. Pharmacol. Ther.* **2011**, *89*, 491–502.
5. Tan, G. R.; Feng, S. S.; Leong, D. T. The Reduction of Anticancer Drug Antagonism by the Spatial Protection of Drugs with PLA-TPGS Nanoparticles. *Biomaterials* **2014**, *35*, 3044–3051.
6. Ganta, S.; Devalapally, H.; Shahiwala, A.; Amiji, M. A Review of Stimuli-Responsive Nanocarriers for Drug and Gene Delivery. *J. Controlled Release* **2008**, *126*, 187–204.
7. Torchilin, V. P. Multifunctional Nanocarriers. *Adv. Drug Delivery Rev.* **2006**, *58*, 1532–1555.
8. Allen, T. M.; Cullis, P. R. Drug Delivery Systems: Entering the Mainstream. *Science* **2004**, *303*, 1818–1822.
9. Liang, X.; Yue, X.; Dai, Z.; Kikuchi, J. Photoresponsive Liposomal Nanohybrid Cerasomes. *Chem. Commun.* **2011**, *47*, 4751–4753.
10. Weinstein, J. N.; Magin, R. L.; Yatvin, M. B.; Zaharko, D. S. Liposomes and Local Hyperthermia: Selective Delivery of Methotrexate to Heated Tumors. *Sciences* **1979**, *204*, 188–191.
11. Alvarez-Lorenzo, C.; Bromberg, L.; Concheiro, A. Light-Sensitive Intelligent Drug Delivery Systems. *Photochem. Photobiol.* **2009**, *85*, 848–860.
12. Tay, C. Y.; Setyawati, M. I.; Xie, J.; Parak, W. J.; Leong, D. T. Back to Basics: Exploiting the Innate Physico-Chemical Characteristics of Nanomaterials for Biomedical Applications. *Adv. Funct. Mater.* **2014**, *24*, 5936–5955.
13. Matsumura, Y.; Maeda, H. A New Concept for Macromolecular Therapeutics in Cancer Chemotherapy: Mechanism of Tumoritropic Accumulation of Proteins and the Antitumor Agent SMANCS. *Cancer Res.* **1986**, *46*, 6387–6392.
14. Maeda, H.; Wu, J.; Sawa, T.; Matsumura, Y.; Hori, K. Tumor Vascular Permeability and the EPR Effect in Macromolecular Therapeutics: A Review. *J. Controlled Release* **2000**, *65*, 271–284.
15. Yu, B.; Tai, H. C.; Xue, W.; Lee, L. J.; Lee, R. J. Receptor Targeted Nanocarriers for Therapeutic Delivery to Cancer. *Mol. Membr. Biol.* **2010**, *27*, 286–298.
16. Setyawati, M. I.; Tay, C. Y.; Chia, S. L.; Goh, S. L.; Fang, W.; Neo, M. J.; Chong, H. C.; Tan, S. M.; Loo, S. C.; Ng, K. W.; et al. Titanium Dioxide Nanomaterials Cause Endothelial Cell Leakiness by Disrupting the Homophilic Interaction of VE-Cadherin. *Nat. Commun.* **2013**, *4*, 1673.
17. Setyawati, M. I.; Tay, C. Y.; Leong, D. T. The Gap between Endothelial Cells: Key to the Quick Escape of Nanomaterials? *Nanomedicine* **2014**, *9*, 1591–1594.
18. Carpentier, A.; Chauvet, D.; Reina, V.; Beccaria, K.; Leclerq, D.; McNichols, R. J.; Gowda, A.; Cornu, P.; Delattre, J. MR-Guided Laser-Induced Thermal Therapy (LITT) for Recurrent Glioblastomas. *Lasers Surg. Med.* **2012**, *44*, 361–368.
19. Fatehi, D.; van der Zee, J.; de Bruijne, M.; Franckena, M.; van Rhoon, G. C. RF-Power and Temperature Data Analysis of 444 Patients With Primary Cervical Cancer: Deep Hyperthermia Using the Sigma-60 Applicator is Reproducible. *Int. J. Hyperthermia* **2007**, *23*, 623–643.
20. Johnson, J. E.; Neuman, D. G.; Maccarini, P. F.; Juang, T.; Stauffer, P. R.; Turner, P. Evaluation of a Dual-Arm Archimedean Spiral Array Formicrowave Hyperthermia. *Int. J. Hyperthermia* **2006**, *22*, 475–490.
21. Salomir, R.; Palussiere, J.; Vimeux, F. C.; de Zwart, J. A.; Quesson, B.; Gauchet, M.; Lelong, P.; Pergrale, J.; Grenier,

N.; Moonen, C. T. Local Hyperthermia with MR-guided Focused Ultrasound: Spiral Trajectory of the Focal Point Optimized for Temperature Uniformity in the Target Region. *J. Magn. Reson. Imaging* **2000**, *12*, 571–583.
22. Hamano, N.; Negishi, Y.; Takatori, K.; Endo-Takahashi, Y.; Suzuki, R.; Maruyama, K.; Niidome, T.; Aramaki, Y. Combination Of Bubble Liposomes and High-Intensity Focused Ultrasound (HIFU) Enhanced Antitumor Effect by Tumor Ablation. *Biol. Pharm. Bull.* **2014**, *37*, 174–177.
23. Morawski, A. M.; Lanza, G. A.; Wickline, S. A. Targeted Contrast Agents for Magnetic Resonance Imaging and Ultrasound. *Curr. Opin. Biotechnol.* **2005**, *16*, 89–92.
24. Unezaki, S.; Maruyama, K.; Takahashi, N.; Koyama, M.; Yuda, T.; Suginaka, A.; Iwatsuru, M. Enhanced Delivery and Antitumor Activity of Doxorubicin Using Long Circulating Thermosensitive Liposomes Containing Amphipathic Polyethylene Glycol in Combination with Local Hyperthermia. *Pharm. Res.* **1994**, *11*, 1180–1185.
25. Gaber, M. H.; Wu, N. Z.; Hong, K.; Huang, S. K.; Dewhirst, M. W.; Papahadjopoulos, D. Thermosensitive Liposomes: Extravasation and Release of Contents in Tumor Microvascular Networks. *Int. J. Radiat. Oncol. Biol. Phys.* **1996**, *36*, 1177–1187.
26. Yatvin, M. B.; Weinstein, J. N.; Dennis, W. H.; Blumenthal, R. Design of Liposomes for Enhanced Local Release of Drugs by Hyperthermia. *Science* **1978**, *202*, 1290–1293.
27. Needham, D.; Anyarambhatla, G.; Kong, G.; Dewhirst, M. W. A New Temperature Sensitive Liposome for Use with Mild Hyperthermia: Characterization and Testing in a Human Tumor Xenograft Model. *Cancer Res.* **2000**, *60*, 1197–1201.
28. Kong, G.; Anyarambhatla, G.; Petros, W. P.; Braun, R. D.; Colvin, O. M.; Needham, D.; Dewhirst, M. W. Efficacy of Liposomes and Hyperthermia in a Human Tumor Xenograft Model: Importance of Triggered Drug Release. *Cancer Res.* **2000**, *60*, 6950–6957.
29. Dromi, S.; Frenkel, V.; Luk, A.; Traughber, B.; Angstadt, M.; Bur, M.; Poff, J.; Xie, J.; Libutti, S. K.; Li, K. C.; et al. Pulsed-High Intensity Focused Ultrasound and Low Temperature-Sensitive Liposomes for Enhanced Targeted Drug Delivery and Antitumor Effect. *Clin. Cancer Res.* **2007**, *13*, 2722–2727.
30. Ponce, A. M.; Vujaskovic, Z.; Yuan, F.; Needham, D.; Dewhirst, M. W. Hyperthermia Mediated Liposomal Drug Delivery. *Int. J. Hyperthermia* **2006**, *22*, 205–213.
31. Koning, G. A.; Eggermont, A. M.; Lindner, L. H.; ten Hagen, T. L. Hyperthermia and Thermosensitive Liposomes for Improved Delivery of Chemotherapeutic Drugs to Solid Tumors. *Pharm. Res.* **2010**, *27*, 1750–1754.
32. Li, L.; ten Hagen, T. L.; Hossann, M.; Süss, R.; van Rhoon, G. C.; Eggermont, A. M.; Haemmerich, D.; Koning, G. A. Mild Hyperthermia Triggered Doxorubicin Release from Optimized Stealth Thermosensitive Liposomes Improves Intratumoral Drug Delivery and Efficacy. *J. Controlled Release* **2013**, *168*, 142–150.
33. Banno, B.; Ickenstein, L. M.; Chiu, G. N.; Bally, M. B.; Thewalt, J.; Brief, E.; Wasan, E. K. The Functional Roles of Poly-(Ethylene Glycol)-Lipid and Lysolipid in the Drug Retention and Release from Lysolipid-Containing Thermosensitive Liposomes *in Vitro* and *in Vivo*. *J. Pharm. Sci.* **2010**, *99*, 2295–2308.
34. Mills, J. K.; Needham, D. Lysolipid Incorporation in Dipalmitoylphosphatidylcholine Bilayer Membranes Enhances the Ion Permeability and Drug Release Rates at the Membrane Phase Transition. *Biochim. Biophys. Acta* **2005**, *1716*, 77–96.
35. Ponce, A. M.; Viglianti, B. L.; Yu, D.; Yarmolenko, P. S.; Michelich, C. R.; Woo, J.; Bally, M. B.; Dewhirst, M. W. Magnetic Resonance Imaging of Temperature-Sensitive Liposome Release: Drug Dose Painting and Antitumor Effects. *J. Natl. Cancer Inst.* **2007**, *99*, 53–63.
36. Landon, C. D.; Park, J. Y.; Needham, D.; Dewhirst, M. W. Nanoscale Drug Delivery and Hyperthermia: the Materials Design and Preclinical and Clinical Testing of Low Temperature-Sensitive Liposomes Used in Combination with Mild Hyperthermia in the Treatment of Local Cancer. *Open Nanomed. J.* **2011**, *3*, 38–64.
37. Needham, D.; Park, J. Y.; Wright, A. M.; Tong, J. Materials Characterization of the Low Temperature Sensitive Liposome (LTSL): Effects of the Lipid Composition (Lysolipid and DSPE-PEG-2000) on the Thermal Transition and Release of Doxorubicin. *Faraday Discuss.* **2013**, *161*, 515–534.
38. de Smet, M.; Langereis, S.; van den Bosch, S.; Grull, H. Temperature-Sensitive Liposomes for Doxorubicin Delivery under MRI Guidance. *J. Controlled Release* **2010**, *143*, 120–127.
39. Woo, J.; Chiu, G. N.; Karlsson, G.; Wasan, E.; Ickenstein, L.; Edwards, K.; Bally, M. B. Use of a Passive Equilibration Methodology to Encapsulate Cisplatin into Preformed Thermosensitive Liposomes. *Int. J. Pharm.* **2008**, *349*, 38–46.
40. Kennedy, J. High-Intensity Focused Ultrasound in the Treatment of Solid Tumours. *Nat. Rev. Cancer* **2005**, *5*, 321–327.
41. Wu, J.; Nyborg, W. L. Ultrasound, Cavitation Bubbles and Their Interaction with Cells. *Adv. Drug Delivery Rev.* **2008**, *60*, 1103–1116.
42. Ranjan, A.; Jacobs, G. C.; Woods, D. L.; Negussie, A. H.; Partanen, A.; Yarmolenko, P. S.; Gacchina, C. E.; Sharma, K. V.; Frenkel, V.; Wood, B. J.; et al. Image-Guided Drug Delivery with Magnetic Resonance Guided High Intensity Focused Ultrasound and Temperature Sensitive Liposomes in a Rabbit Vx2 Tumor Model. *J. Controlled Release* **2012**, *158*, 487–494.
43. Gasselhuber, A.; Dreher, M. R.; Partanen, A.; Yarmolenko, P. S.; Woods, D.; Wood, B. J.; Haemmerich, D. Targeted Drug Delivery by High Intensity Focused Ultrasound Mediated Hyperthermia Combined with Temperature-Sensitive Liposomes: Computational Modelling and Preliminary *in Vivo* Validation. *Int. J. Hyperthermia* **2012**, *28*, 337–348.
44. de Smet, M.; Heijman, E.; Langereis, S.; Hijnen, N. M.; Grüll, H. Magnetic Resonance Imaging of High Intensity Focused Ultrasound Mediated Drug Delivery from Temperature-Sensitive Liposomes: An *in Vivo* Proof-of-Concept Study. *J. Controlled Release* **2011**, *150*, 102–110.
45. Partanen, A.; Yarmolenko, P. S.; Viitala, A.; Appanaboyina, S.; Haemmerich, D.; Ranjan, A.; Jacobs, G.; Woods, D.; Enholm, J.; Wood, B. J.; et al. Mild Hyperthermia with Magnetic Resonance-Guided High-Intensity Focused Ultrasound for Applications in Drug Delivery. *Int. J. Hyperthermia* **2012**, *28*, 320–336.
46. Grüll, H.; Langereis, S. Hyperthermia-Triggered Drug Delivery from Temperature Sensitive Liposomes Using MRI-Guided High Intensity Focused Ultrasound. *J. Controlled Release* **2012**, *161*, 317–327.
47. Staruch, R.; Chopra, R.; Hynynen, K. Localised Drug Release Using MRI-Controlled Focused Ultrasound Hyperthermia. *Int. J. Hyperthermia* **2011**, *27*, 156–171.
48. Park, S. M.; Kim, M. S.; Park, S. J.; Park, E. S.; Choi, K. S.; Kim, Y. S.; Kim, H. R. Novel Temperature-Triggered Liposome with High Stability: Formulation, *in Vitro* Evaluation, and *in Vivo* Study Combined with High-Intensity Focused Ultrasound (HIFU). *J. Controlled Release* **2013**, *170*, 373–379.
49. Changsan, N.; Chan, H.-K.; Separovic, F.; Srichana, T. Physicochemical Characterization and Stability of Rifampicin Liposome Dry Powder Formulations for Inhalation. *J. Pharm. Sci.* **2009**, *98*, 628–639.
50. Behera, T.; Swain, P.; Sahoo, S. K. Antigen in Chitosan Coated Liposomes Enhances Immune Responses Through Parenteral Immunization. *Int. Immunopharmacol.* **2011**, *11*, 907–914.
51. Poon, R. T.; Borys, N. Lyso-Thermosensitive Liposomal Doxorubicin: a Novel Approach to Enhance Efficacy of Thermal Ablation of Liver Cancer. *Expert Opin. Pharmacother.* **2009**, *10*, 333–343.
52. Gasselhuber, A.; Dreher, M. R.; Negussie, A.; Wood, B. J.; Rattay, F.; Haemmerich, D. Mathematical Spatio-Temporal Model of Drug Delivery from Low Temperature Sensitive Liposomes During Radiofrequency Tumour Ablation. *Int. J. Hyperthermia* **2010**, *26*, 499–513.
53. Negussie, A. H.; Yarmolenko, P. S.; Partanen, A.; Ranjan, A.; Jacobs, G.; Woods, D.; Bryant, H.; Thomasson, D.;

Dewhirst, M. W.; Wood, B. J.; et al. Formulation and Characterisation of Magnetic Resonance Imageable Thermally Sensitive Liposomes for Use With magnetic Resonance-Guided High Intensity Focused Ultrasound. *Int. J. Hyperthermia* **2011**, *27*, 140–155.
54. Cao, Z.; Ma, Y.; Yue, X.; Li, S.; Dai, Z.; Kikuchi, J. Stabilized Liposomal Nanohybrid Cerasomes for Drug Delivery Applications. *Chem. Commun.* **2010**, *46*, 5265–5267.
55. Kawataki, T.; Yasuhara, K.; Kikuchi, J. Remarkable Long-Term Stability of Cerasome as an Organicinorganic Hybrid Nanocontainer for Water-Soluble Macromolecules. *Chem. Lett.* **2011**, *40*, 461–463.
56. Ma, Y.; Dai, Z.; Gao, Y.; Cao, Z.; Zha, Z.; Yue, X.; Kikuchi, J. Liposomal Architecture Boosts Biocompatibility of Nanohybrid Cerasomes. *Nanotoxicology* **2011**, *5*, 622–635.
57. Jin, Y.; Yue, X.; Zhang, Q.; Wu, X.; Cao, Z.; Dai, Z. Cerasomal Doxorubicin With Long-Term Storage Stability and Controllable Sustained Release. *Acta Biomater.* **2012**, *8*, 3372–3380.
58. Cao, Z.; Yue, X.; Jin, Y.; Wu, X.; Dai, Z. Modulation of Release of Paclitaxel from Composite Cerasomes. *Colloids Surf., B* **2012**, *98*, 97–104.
59. Liang, X.; Li, X.; Jing, L.; Xue, P.; Jiang, L.; Ren, Q.; Dai, Z. Design and Synthesis of Lipidic Organoalkoxysilane for Self-assembly of Liposomal Nanohybrid Cerasomes with Controlled Drug Release Properties. *Chem.—Eur. J.* **2013**, *19*, 16113–16121.
60. Yue, X.; Dai, Z. Recent Advances in Liposomal Nanohybrid Cerasomes as Promising Drug Nanocarriers. *Adv. Colloid Interface Sci.* **2014**, *207*, 32–42.
61. Mills, J. K.; Needham, D. The Materials Engineering of Temperature-Sensitive Liposomes. *Methods Enzymol.* **2004**, *387*, 82–113.
62. Hristova, K. A. D. N. Influence of Bilayer Fluctuations on the Steric Interactions Between Polymer-Grafted Bilayers. *Liq. Cryst.* **1995**, *18*, 423–430.
63. May, J. P.; Li, S. D. Hyperthermia-Induced Drug Targeting. *Expert Opin. Drug Delivery* **2013**, *10*, 511–527.
64. Park, C.; Lim, J.; Yun, M.; Kim, C. Photoinduced Release of Guest Molecules by Supramolecular Transformation of Self-Assembled Aggregates Derived from Dendrons. *Angew. Chem., Int. Ed.* **2008**, *47*, 2959–2963.
65. Chen, D.; Wu, J. An *in Vitro* Feasibility Study of Controlled Drug Release from Encapsulated Nanometer Liposomes Using High Intensity Focused Ultrasound. *Ultrasonics* **2010**, *50*, 744–749.
66. Juliano, R. L.; Stamp, D. The Effect of Particle Size and Charge on the Clearance Rates of Liposomes and Liposome Encapsulated Drugs. *Biochem. Biophys. Res. Commun.* **1975**, *63*, 651–658.
67. Sheng, Y.; Liu, C.; Yuan, Y.; Tao, X.; Yang, F.; Shan, X.; Zhou, H.; Xu, F. Long-Circulating Polymeric Nanoparticles Bearing a Combinatorial Coating of PEG and Water-Soluble Chitosan. *Biomaterials* **2009**, *30*, 2340–2348.
68. He, C.; Hu, Y.; Yin, L.; Tang, C.; Yin, C. Effects of Particle Size and Surface Charge on Cellular Uptake and Biodistribution of Polymeric Nanoparticles. *Biomaterials* **2010**, *31*, 3657–3666.
69. Roser, M.; Fischer, D.; Kissel, T. Surface-Modified Biodegradable Albumin Nano and Microspheres. II: Effect of Surface Charges on *in Vitro* Phagocytosis and Biodistribution in Rats. *Eur. J. Pharm. Biopharm.* **1998**, *46*, 255–263.
70. Hu, C. S.; Chiang, C. H.; Hong, P. D.; Yeh, M. K. Influence of Charge on FITC-BSA-Loaded Chondroitin Sulfate-chitosan Nanoparticles upon Cell Uptake in Human Caco-2 Cell Monolayers. *Int. J. Nanomed.* **2012**, *7*, 4861–4872.
71. Xiao, K.; Li, Y.; Luo, J.; Lee, J. S.; Xiao, W.; Gonik, A. M.; Agarwal, R. G.; Lam, K. S. The Effect of Surface Charge on *in Vivo* Biodistribution of PEG-oligocholic Acid Based Micellar Nanoparticles. *Biomaterials* **2011**, *32*, 3435–3446.
72. Dobrovolskaia, M. A.; Aggarwal, P.; Hall, J. B.; McNeil, S. E. Preclinical Studies To Understand Nanoparticle Interaction with the Immune System and Its Potential Effects on Nanoparticle Biodistribution. *Mol. Pharmaceutics* **2008**, *5*, 487–495.
73. Liberman, A.; Wu, Z.; Barback, C. V.; Viveros, R. D.; Wang, J.; Ellies, L. G.; Mattrey, R. F.; Trogler, W. C.; Kummel, A. C.; Blair, S. L. Hollow Iron-Silica Nanoshells for Enhanced High Intensity Focused Ultrasound. *J. Surg. Res.* **2014**, *190*, 391–398.
74. Wang, X.; Chen, H.; Zheng, Y.; Ma, M.; Chen, Y.; Zhang, K.; Zeng, D.; Shi, J. Au-Nanoparticle Coated Mesoporous Silica Nanocapsule-Based Multifunctional Platform for Ultrasound Mediated Imaging, Cytoclasis and Tumor Ablation. *Biomaterials* **2013**, *34*, 2057–2068.
75. Setyawati, M. I.; Kutty, R. V.; Tay, C. Y.; Yuan, X.; Xie, J.; Leong, D. T. Novel Theranostic DNA Nanoscaffolds for the Simultaneous Detection and Killing of *Escherichia coli* and *Staphylococcus aureus*. *ACS Appl. Mater. Interfaces* **2014**, *6*, 21822–21831.
76. Phillips, L. C.; Puett, C.; Sheeran, P. S.; Wilson Miller, G.; Matsunaga, T. O.; Dayton, P. A. Phase-Shift Perfluorocarbon Agents Enhance High Intensity Focused Ultrasound Thermal Delivery with Reduced Near-field Heating. *J. Acoust. Soc. Am.* **2013**, *134*, 1473–1482.
77. Chen, K. J.; Liang, H. F.; Chen, H. L.; Wang, Y.; Cheng, P. Y.; Liu, H. L.; Xia, Y.; Sung, H. W. A Thermoresponsive Bubble-Generating Liposomal System for Triggering Localized Extracellular Drug Delivery. *ACS Nano* **2013**, *7*, 438–446.
78. Ma, Y.; Liang, X.; Tong, S.; Bao, G.; Ren, Q.; Dai, Z. Gold Nanoshelled Nanomicelles for Potential MRI Imaging, Light-Triggered Drug Release and Photothermal Therapy. *Adv. Funct. Mater.* **2013**, *23*, 815–822.
79. Jalota, S.; Bhaduri, S. B.; Tas, A. C. Using a Synthetic Body Fluid (SBF) Solution of 27 mM $HCO_3^-$ To Make Bone Substitutes More Osteointegrative. *Mater. Sci. Eng., C* **2008**, *28*, 129–140.